

Band Profile and Surface Acoustic Wave Attenuation Analysis of Polygonal Cavity-type Piezoelectric Phononic Crystals

F. Kuruoğlu^{1*}, N. S. Genç¹, A. Erol¹, and A. Çiçek²

¹Istanbul University, Faculty of Science, Department of Physics, Vezneciler, 34134, Istanbul, Türkiye

²Burdur Mehmet Akif Ersoy University, Faculty of Arts and Science, Department of Nanoscience and Nanotechnology, 15030, Burdur, Türkiye

ABSTRACT

In this study, we examined the dispersion profiles and surface acoustic wave attenuation properties of polygonal cavity-type phononic crystals in relation to changes in the number of vertices. Both band analysis and transmission spectrum calculations are performed using finite element method simulations. The findings indicate an increase in the number of vertices of phononic crystal results in an increase in local resonance bandgap frequencies and corresponding transmission peaks. Furthermore, the phononic crystal bandgap widens from 7.3 MHz to 11.1 MHz as the number of vertices increases from 3 to 14, as demonstrated by the obtained dispersion profiles. Comparable features are observed in the transmission spectra for alternating polygonal cavity-type phononic crystal periodic grooves. Additionally, the ability of the surface acoustic wave attenuation is affected by the phononic crystal shape, and the resonance frequency of the phononic crystals can be adjusted by changing the number of vertices.

Keywords: Surface acoustic wave – phononic crystal – metasurface – Finite element method – phononic bandgap

1. INTRODUCTION

The ability to manipulate biological or inorganic objects without physical contact has long been a desired goal. Electromagnetic and acoustic waves have emerged as the most effective means to achieve this aim (Collins et al. 2016). Surface acoustic waves (SAWs) have gained significant attention in various research and application areas, including delay lines (Topaltzikis et al. 2021), filters (Su et al. 2021b,a), microfluidics (Xie et al. 2020; Qian et al. 2020; Agostini et al. 2019), gas-detection (Kumar & Prajesh 2022; Hekiem et al. 2021), mass detection (Wang et al. 2019), and bio-detection (Zhang et al. 2015; Kidakova et al. 2020) applications. The widespread use of SAW devices arises from their versatility across different fields of research and application. Phononic crystals (PnCs) are structures that offer acoustic bandgaps based on the material's periodicity and geometry, similar to photonic crystal slabs (Kushwaha et al. 1994; Sigalas & Economou 1993; Mead 1996; Kushwaha et al. 1993; Guo et al. 2023; Li et al. 2020). Pillar arrays have emerged as the most prominent geometry for PnCs, with a broad range of application areas (Achaoui et al. 2011, 2013; Jin et al. 2021). Piezoelectric phononic crystals (PPnCs) have also gained attention due to their physical properties and applications in waveguiding (Oh et al. 2011; Vasseur et al. 2007; Zhang et al. 2020; Korozlu et al. 2022), bio and mass sensing (Gharibi et al.

2019; Gharibi & Mehaneq 2021; Schmidt et al. 2016), energy harvesting (Cao et al. 2019), and microfluidics (Bourquin et al. (2011)). The geometric parameters of PPnCs, such as locally resonance and/or Bragg bandgap, determine their performance and versatility.

Recent studies have shown that using cavity-shaped metamaterials as piezoelectric phononic crystals can lead to broader SAW bandgaps (Ash et al. 2017; Pouya & Nash 2021). The geometrical parameters, including cavity radius, pillar height, and groove depth, play a crucial role in determining the frequency range where the phononic crystal will be effective (Kuruoğlu 2022). Therefore, obtaining the proper geometrical parameters and understanding their effects on the acoustic bandgap is crucial for superior phononic device applications.

In this paper, we introduce the band profile and the SAW attenuation characteristics of the PPnCs, which have been modelled with the various number of vertices from $n=3$ to $n=14$. A series of Finite Element Method (FEM) simulations were conducted to analyze and correlate the acoustic field behaviour based on the number of pillar vertices of the PPnCs by using the *COMSOL Multiphysics Software*.

Corresponding Author: F. Kuruoğlu E-mail: furkan.kuruoglu@istanbul.edu.tr

Submitted: 28.04.2023 • Revision Requested: 17.05.2023 • Last Revision Received: 19.05.2023 • Accepted: 22.05.2023 • Published Online: 25.05.2023



This article is licensed under a Creative Commons Attribution-NonCommercial 4.0 International License (CC BY-NC 4.0)

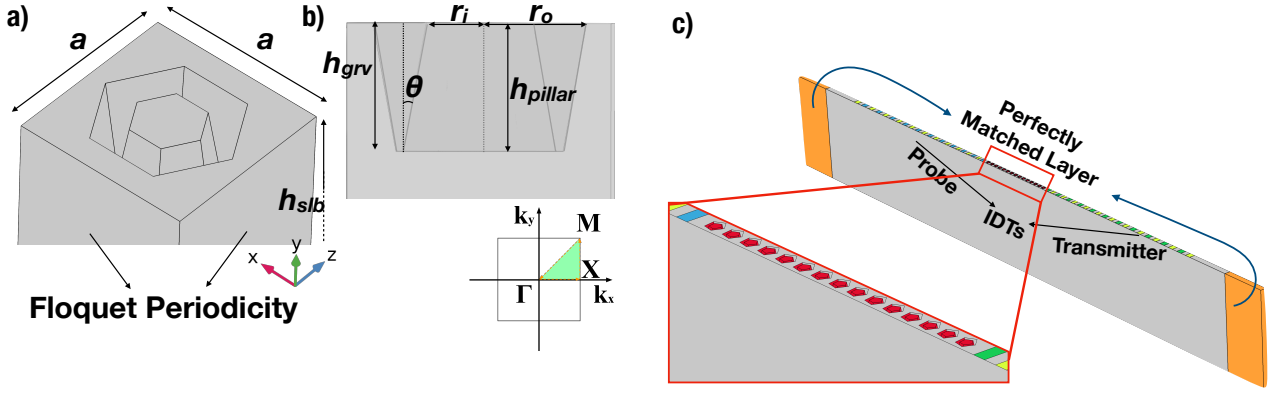


Figure 1. a) 3D unit cell used for the simulation of the band profile, b) Cross-sectional view of the unit cell and the wavevector path for the square arrayed PPnCs and c) the 3D FEM model that simulated the SAW attenuation characteristics of the PPnC array.

2. METHODS

To examine the band structures of polygonal cavity-type PPnCs and SAW transmission spectra with different numbers of PPnC vertices, FEM simulations were conducted. These simulations utilized *COMSOL Multiphysics* 6.1, which incorporates the piezoelectricity module to couple the elastic wave equation and Maxwell's related equation (Gauss' law). This allows the determination of stresses and electrical potential distributions over piezoelectric materials.

To facilitate a comparison with the research conducted by [Ash et al. \(2017\)](#), a two-dimensional (2D) PPnC in the form of a square lattice was utilized. As depicted in Figure 1a, the square arrayed PPnCs were modelled by fixing the groove depth (h_{grv}) to $6\mu\text{m}$, groove top radius (r_o) to $5\mu\text{m}$, pillar bottom radius (r_i) to $3\mu\text{m}$, and lattice constant (a) to $12\mu\text{m}$. The pillar height (h_{pillar}) was defined as the same as the groove depth. The wall inclination angle (θ) was set to $10^\circ.2$, which has been experimentally reported for 128° Y-cut X-propagating (YX- 128°) lithium niobate (LiNbO_3) ([Yavuzcetin et al. 2011](#)). This cut was defined in *COMSOL* using Euler angles $(\alpha, \beta, \gamma) = (0, 38^\circ, 0)$. The use of Euler angles is more convenient than the transformation of elasticity and coupling matrices of Z-cut LiNbO_3 .

To determine the eigenfrequencies of the polygonal cavity-type PPnCs and their corresponding transmission spectra as a function of the number of vertices, FEM simulations were conducted on the irreducible Brillouin zone (BZ) in the first BZ, with the wavevector \mathbf{k} being swept along the $\Gamma \rightarrow X \rightarrow M \rightarrow \Gamma$ path for the square array. A 3D schematic of the modelled PPnC unit cell is depicted in Figure 1b, where Bloch-Floquet periodic boundary condition (PBC) was defined for both opposing sides of the unit cell, and the bottom side of the unit cell was defined as a fixed constraint surface. The piezoelectric slab height was set to $h_{slb} = 200\mu\text{m}$, and the local resonance bandgap (LRBG) resulting from the resonance vibrations of the core column was found to be below the expected Bragg bandgap [19]. The

LRBG edge frequencies and width can be adjusted by varying the number of vertices of the PPnCs.

To obtain the transmission spectra for each number of vertices, frequency domain FEM simulations were conducted to generate Rayleigh-type SAWs using interdigitated transducers (IDTs) as the standard means of radio frequency (RF) SAW generation. The SAW transmission spectra were simulated for two facing identical IDTs and a PPnC array in between, as shown in Figure 1c. To work in a broad frequency range, chirped IDTs were modelled with a finger width range of $7.5\mu\text{m}$ to $12.5\mu\text{m}$, with a step increase of $\Delta\omega = 0.5\mu\text{m}$, and the number of finger pairs in each IDT set to $N_{IDT} = 11$. The PPnC array consisted of 15 periodic units equally spaced from the IDT fingers, lying along the [10] direction. The IDT on the left was defined as the source to propagate SAW, while the right-side IDT was used to probe the transmitted signal through the floating potential (V_{probe}). SAW transmittance (S_{21}) was calculated using the $S_{21} = 20 \times \log_{10}(V_{probe}/V_{applied})$ where $V_{applied} = 50\text{ V}$ was the RF amplitude ([Ulug et al. 2022](#)). To minimize unwanted reflections, low-reflecting boundaries (LRB) were placed on the bottom side of the model, and perfectly matched layers (PML) were placed at the edges of the model in the direction of SAW propagation. Periodic boundary conditions (PBC) were used for the sides parallel to the SAW propagation direction, allowing only one row of the PPnC to be modelled while the rest were replicated infinitely through the PBC.

3. RESULTS

The band profiles of triangular ($n=3$) and tetradecagonal cavity-shaped PPnCs, which represent the two external investigated cases in the present work, were plotted as can be seen in Figure 2a and b, respectively. The red dashed lines represent the Rayleigh SAW modes of the bulk slab without perturbation, while the dispersion lines of other leaky SAW modes are omitted. The shaded regions in red and green indicate the excluded

ranges of these leaky modes. The two lowest bands are associated with the bending and expansion modes of the core pillar, and hence, they are flat as stated in Jin et al. (2021). In contrast, the third band consists of the anti-resonant modes of the outer grooves. So all these modes are labelled as A, B and C, respectively and the corresponding displacements were given as inset in Figure 2.

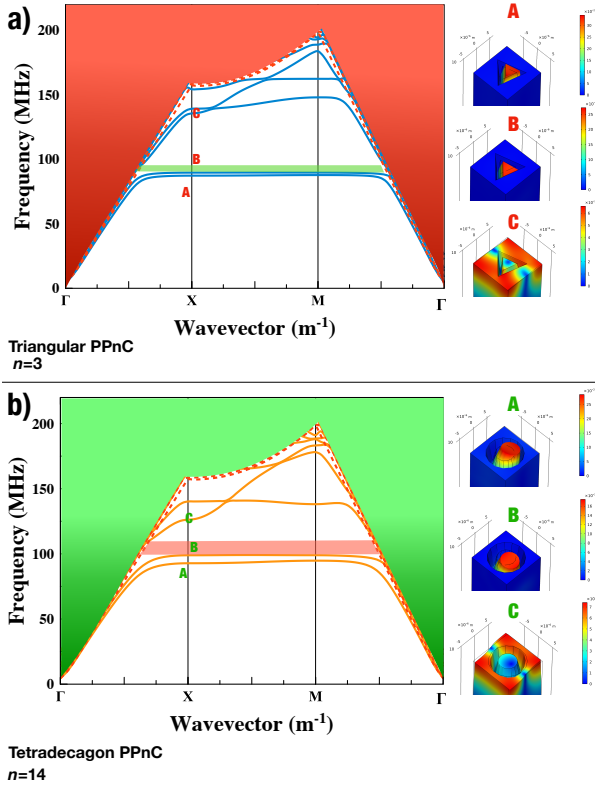


Figure 2. Band profile of a) triangular ($n=3$) cavity type and b) tetradecagon ($n=14$) type PPnC and corresponding displacements in the resonance frequencies.

The horizontal hatched highlighted stripes in Figure 2a and b represent the local resonance bandgap region of the PPnC unit cell. As the number of vertices increases, the LRBG broadens and its central frequency f_c is shifted to higher values.

In order to obtain an explicit knowledge of the effect of the number of vertices in the band profile, a series of band profiles were studied from $n=3$ to $n=14$ where the n is the number of vertices. In Figure 3, band behaviours in the BZ were plotted for each PPnC vertices type. The LRBG-related bands shift to the higher frequencies up to $n=6$, while no band profile change was observed afterward.

The BG characteristics as a function of the number of vertices were plotted as in Figure 4a to bring clarity to the geometry dependence of the polygonal cavity-type PPnCs. The corresponding frequencies to the BG edges shift to the higher-frequency regions with the increasing number of vertices and remain almost fixed for the greater edge number than $n=6$. This behaviour can be attributed to changes in the moment of inertia

(ΔI) with respect to the polygonal cavity shape (Muhammad et al. 2021; Tateno et al. 2021; Guo & Zhang 2022). Figure 4b was plotted to emphasize the coherence of the frequency response and the moment of inertia of the polygonal cavity type PPnCs. The moment of inertia difference, which equals to the moment of inertia of the cavity, represents the same trend as the resonance frequencies. It is also stated from the 1st derivatives of the moment of inertia and mass of the cavity as can be seen in Figure 4c, the governing factor is the extracted mass for both moments of inertia and the resonance frequency.

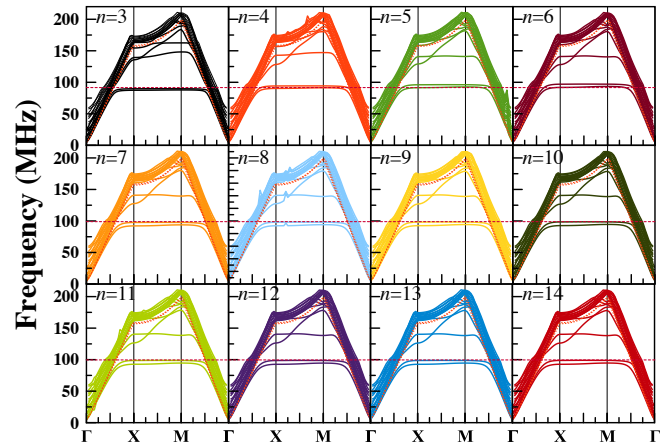


Figure 3. The band structures of the square array polygonal cavity-type PPnCs for the different number of vertices.

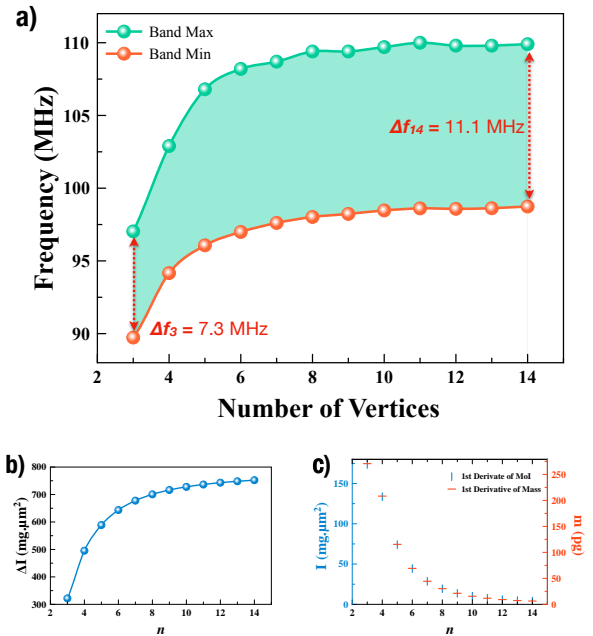


Figure 4. a) Changes in the frequencies at the edges of the LRBG with respect to the number of vertices of polygonal cavity-type PPnC, b) the moment of inertia difference (ΔI) of groove and pillar as a function of the number of vertices that equals to the extracted part to create the cavity and c) 1st derivatives of the moment of inertia and mass of the extracted part of the polygonal cavity-type PPnC.

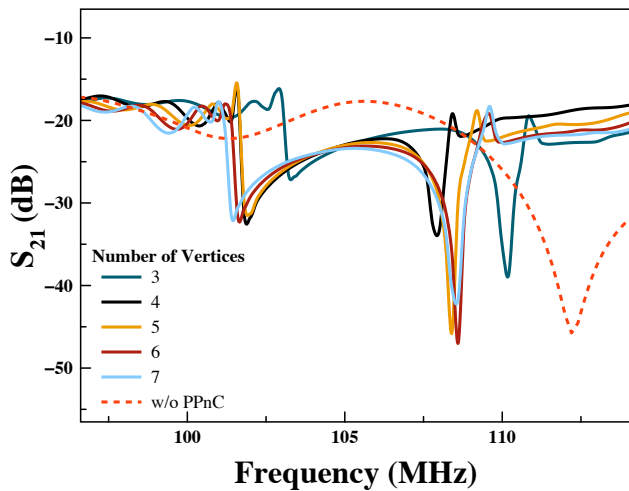


Figure 5. Transmission spectra of SAWs are presented for the polygonal cavity-type square PPnC array with varying numbers of vertices oriented along the [10] direction.

To gain a better understanding of the interaction between PPnC and SAW, transmission spectra (S_{21}) were obtained. Figure 5 displays the SAW transmission spectra in the range of 95 MHz to 115 MHz for each number of vertices ranging from 3 to 7. The red dashed line in Figure 5 represents the S_{21} spectrum of the bare chirped IDT pairs without the PPnC between them. Each transmission spectrum shows two distinct peaks, with the major peak at approximately 107 MHz and the minor peak at around 102 MHz. In comparison to the dispersion profiles, both S_{21} peak intensities increase until the number of vertices is $n=6$. Once the number of vertices increases, the peak intensity around 107 MHz decreases, which results in a poorer SAW attenuation performance. Besides, the minor peak intensity remains almost constant for each PPnC geometry. Also, the major peak frequency shifts through the higher frequencies, as stated in the band profile characteristics.

4. CONCLUSION

To summarize, the simulation results of band structures and SAW transmission spectra for polygonal cavity-type PPnCs are presented as a function of the number of vertices of the PPnC. The LRBG edge frequencies increase, and the width of LRBG increases as the number of vertices of PPnC increases. The attenuation profile tends to increase with the increasing number of vertices of PPnC, and also, the peak frequency shifts through to the higher frequencies up to $n=6$. All these characterised properties of the polygonal cavity-type PPnCs were reasoned by the changing extracted mass amount to create different polygonal-shaped cavities, and that makes the investigated PPnCs suitable for sensing applications through the mass loading effect while PPnCs exhibit overt characteristic responses to the sub-nano gram mass differences.

Peer Review: Externally peer-reviewed.

Author Contribution: Conception/Design of study - F.K.; Data Acquisition - F.K., N.S.G.; Data Analysis/Interpretation - F.K., N.S.G., A.E., A.Ç.; Drafting Manuscript - F.K., N.S.G., A.E., A.Ç.; Critical Revision of Manuscript - F.K., N.S.G., A.E., A.Ç.; Final Approval and Accountability - F.K., A.E., A.Ç.; Supervision - A.E., A.Ç.

Conflict of Interest: Authors declared no conflict of interest.

Financial Disclosure: Authors declared no financial support.

ACKNOWLEDGEMENTS

This work is funded by The Scientific and Technological Research Council of Turkey (TÜBİTAK) (Project No: 120F337).

LIST OF AUTHOR ORCIDS

F. Kuruoğlu <https://orcid.org/0000-0002-5314-4441>
 N. S. Genç <https://orcid.org/0009-0001-5301-177X>
 A. Erol <https://orcid.org/0000-0003-4196-1791>
 A. Çiçek <https://orcid.org/0000-0002-7686-0045>

REFERENCES

- Achaoui Y., Khelif A., Benchabane S., Robert L., Laude V., 2011, *Physical Review B*, 83, 104201
 Achaoui Y., Laude V., Benchabane S., Khelif A., 2013, *Journal of Applied Physics*, 114, 104503
 Agostini M., Greco G., Cecchini M., 2019, *IEEE Access*, 7, 70901
 Ash B. J., Worsfold S. R., Vukusic P., Nash G. R., 2017, *Nature Communications*, 8, 174
 Bourquin Y., Wilson R., Zhang Y., Reboud J., Cooper J. M., 2011, *Advanced Materials*, 23, 1458
 Cao D., Hu W., Gao Y., Guo X., 2019, *Smart Materials and Structures*, 28, 085014
 Collins D. J., Devendran C., Ma Z., Ng J. W., Neild A., Ai Y., 2016, *Science Advances*, 2, e1600089
 Gharibi H., Mehaney A., 2021, *Physica E: Low-dimensional Systems and Nanostructures*, 126, 114429
 Gharibi H., Khaligh A., Bahrami A., Ghavifekr H. B., 2019, *Journal of Molecular Liquids*, 296, 111878
 Guo J. C., Zhang Z., 2022, *Applied Physics A*, 128, 126
 Guo L., Zhao S., Guo Y., Yang J., Kitipornchai S., 2023, *International Journal of Mechanical Sciences*, 240, 107956
 Hekiem N. L. L., Ralib A. A. M., Hattar M. A. b. M., Ahmad F., Nordin A. N., Rahim R. A., Za'bah N. F., 2021, *Sensors and Actuators A: Physical*, 329, 112792
 Jin Y., Pennec Y., Bonello B., Honarvar H., Dobrzynski L., Djafari-Rouhani B., Hussein M. I., 2021, *Reports on Progress in Physics*, 84, 086502
 Kidakova A., Boroznjak R., Reut J., Öpik A., Saarma M., Syritski V., 2020, *Sensors and Actuators B: Chemical*, 308, 127708
 Korozlu N., Biçer A., Sayarcan D., Kaya O. A., Cicek A., 2022, *Ultrasonics*, 124, 106777

- Kumar A., Prajesh R., 2022, *Sensors and Actuators A: Physical*, p. 113498
- Kuruoğlu F., 2022, *Cumhuriyet Science Journal*, 43, 346
- Kushwaha M. S., Halevi P., Dobrzynski L., Djafari-Rouhani B., 1993, *Physical Review Letters*, 71, 2022
- Kushwaha M. S., Halevi P., Martínez G., Dobrzynski L., Djafari-Rouhani B., 1994, *Physical Review B*, 49, 2313
- Li X., Ning S., Liu Z., Yan Z., Luo C., Zhuang Z., 2020, *Computer Methods in Applied Mechanics and Engineering*, 361, 112737
- Mead D., 1996, *Journal of Sound and Vibration*, 190, 495
- Muhammad Lim C., Leung A. Y. T., 2021, *Acoustics*, 3, 25
- Oh J. H., Lee I. K., Ma P. S., Kim Y. Y., 2011, *Applied Physics Letters*, 99, 083505
- Pouya C., Nash G. R., 2021, *Communications Materials*, 2, 55
- Qian J., Ren J., Liu Y., Lam R. H. W., Lee J. E.-Y., 2020, *Analyst*, 145, 7752
- Schmidt M.-P., Oseev A., Lucklum R., Zubtsov M., Hirsch S., 2016, *Microsystem Technologies*, 22, 1593
- Sigalas M., Economou E., 1993, *Solid State Communications*, 86, 141
- Su R., et al., 2021a, *IEEE Transactions on Device and Materials Reliability*, 21, 365
- Su R., et al., 2021b, *IEEE Electron Device Letters*, 42, 438
- Tateno S., Kurimune Y., Matsuo M., Yamanoi K., Nozaki Y., 2021, *Physical Review B*, 104, L020404
- Topaltzikis D., et al., 2021, *Applied Physics Letters*, 118, 133501
- Ulug B., Kuruoğlu F., Yalçın Y., Erol A., Sarcan F., Şahin A., Cicek A., 2022, *Journal of Physics D: Applied Physics*, 55, 225303
- Vasseur J. O., Hladky-Hennion A.-C., Djafari-Rouhani B., Duval F., Dubus B., Pennec Y., Deymier P. A., 2007, *Journal of Applied Physics*, 101, 114904
- Wang Y., Wang Y., Liu W., Chen D., Wu C., Xie J., 2019, *Sensors and Actuators A: Physical*, 288, 67
- Xie Y., Mao Z., Bachman H., Li P., Zhang P., Ren L., Wu M., Huang T. J., 2020, *Journal of biomechanical engineering*, 142
- Yavuzcetin O., Ozturk B., Xiao D., Sridhar S., 2011, *Optical Materials Express*, 1, 1262
- Zhang X.-F., Zhang Z.-W., He Y.-L., Liu Y.-X., Li S., Fang J.-Y., Zhang X.-A., Peng G., 2015, *Frontiers of Physics*, 11
- Zhang Z.-D., Liu F.-K., Yu S.-Y., Lu M.-H., Chen Y.-F., 2020, *Applied Physics Express*, 13, 044002